Advances in Natural Sciences: Nanoscience and Nanotechnology

Selective and reversible carbon mono oxide gas detection using silver doped octahedral molecular sieves (OMS-2) nanorods

Adv. Nat. Sci.: Nanosci. Nanotechnol. **15** (2024) 035008 (8pp) https://doi.org/10.1088/2043-6262/ad6cc4

Selective and reversible carbon mono oxide gas detection using silver doped octahedral molecular sieves (OMS-2) nanorods

Amit Kumar Gupta[1], Priyanshu Singh[1], Monica Jaiswal[1], Jagjiwan Mittal[1], Sivanandam Aravindan[2], Sumit Chaudhary[3], Satinder Kumar Sharma[3] and Robin Kumar[1]

[1] Amity Institute of Nanotechnology, Amity University, Noida Sector 125, Uttar Pradesh 201301, India
[2] Indian Institute of Technology, Delhi−110016, India
[3] Indian Institute of Technology, Mandi−110016, India

E-mail: rkumar5@amity.edu

Received 23 November 2023
Accepted for publication 26 March 2024
Published 22 August 2024

Abstract

In this work a potable, resistive sensor is fabricated for the selective detection of CO gas using nanorods of Ag doped octahedral molecular sieves-2 (Ag-OMS-2). During exposure to carbon monoxide (CO) gas at room temperature, resistance of Ag-OMS-2 film was dropped from 557 kΩ to 352 kΩ in just 18 sec. However, exposed sample regained its initial resistance value in 25 sec when CO gas source was removed. Both sensing and recovery processes were carried out at room temperature. The sensor film showed excellent reproducibility during several cycles of CO gas exposure. Swift activation of oxygen molecules for the oxidation of CO by the silver present in the tunnel of manganese oxide network is supposed to be responsible for sensing activity of Ag-OMS-2 towards carbon monoxide gas.

Keywords: resistive gas sensor, Ag-OMS-2, thin film, carbon monoxide, gas sensor, nanorods
Classification numbers: 2.01, 5.06, 6.08

1. Introduction

Due effect of environmental pollution on the health of humans, monitoring of polluted gases such as NH_3, CO, NO_2, H_2S etc is the highest priorities of the government agencies. Many studies are carried out for the using different materials for these polluted gases [1–5].

Globally carbon monoxide (CO) is a major pollutant in our atmosphere due to its extreme toxicity. As per the global recommendations limit of CO gas exposure for work must be <35 ppm concentration in air. Beyond this limit CO gas causes various health issues to humans and livestock and its high concentrations may cause unconsciousness and death [6]. So, there is an utmost need for developing a low cost, extremely selective and precise sensor for CO gas. The main aim remains to achieve the best CO gas sensing performance in terms of superior selectivity, sensitivity, squat response, and recovery time by means of different materials and methods [7].

Oxides of semiconducting metals have been extensively studied for the development of CO gas sensors [8, 9]. It was reported in earlier studies that the CO oxidation activity of transition metal oxides would be enhanced while doping them with precious metals such as Ag [10] or Au [11] in Fe_2O_3. Adsorption of CO and O_2 could be propped up by the Schottky effects between metal and metal oxide. This leads towards the development of economical metal oxide catalysts as an alternative to costly metal catalysts for the oxidation of CO oxidation. Manganese oxide octahedral molecular sieves (OMS-2) have been extensively studied, since it provides high stability, along with easy synthesis and cost effective processing. It also offers appreciable catalytic activity. It is known to be highly appropriate for their applications in gas sensing [4, 5]. Their high specific surface area is responsible for the adsorption for gases, making it highly sensitive. The K-OMS-2 is an effectual green oxidation catalyst [12, 13].

Applications of K-OMS-2 are enhanced after doping with metals (M-OMS-2). Small amount of metal doping alters

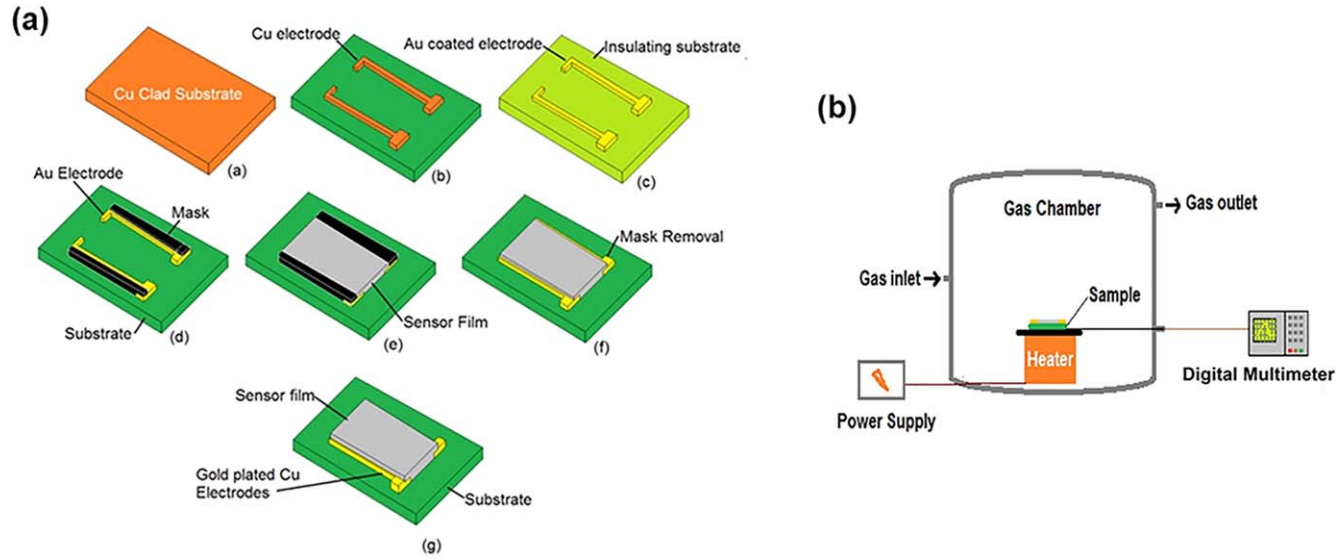

Figure 1. (a)–(d) Fabrcation process of Au coated Cu electrodes on a Cu clad substrate using photolithography, (e) and (f) depositing thin film of Ag-OMS-2 nanorods between two electrodes using hard mask (g) final device used for carbon monoxide gas sensing (b) Gas sensing measurement set up.

chemical and physical properties of K-OMS-2 nanorods. This increases the specific surface area and improves the catalytic properties for adsorbing larger number of gas molecules. These nanorods have been primarily used in catalytic oxidation of various pollutants e.g.CO [14–16], phenol [17], methanol [18], cyclohexanol [19], ammonia [10, 12] and VOCs [20, 21]. In our previous work we have established the gas sensing applications of Cu and Nb doped K-OMS-2 nano fibres [22, 23]. Ag-OMS-2 has been reported as a catalyst for CO oxidation and showed the conversion of 30%–40% below 40 °C [24].

In the current study, Ag doped K-OMS-2 (Ag-OMS-2) was prepared after doping the Ag into K-OMS-2 fibres using a simple method. As prepared Ag-OMS-2 was then studied for the sensing of Carbon monoxide. Synthesis of Ag-OMS-2 using various characterization methods and its application for CO gas sensing along with mechanism are discussed in the paper.

2. Experimental

2.1. Materials/chemicals

The high purity and analytical grade were of analytical grade, $KMnO_4$ (potassium permanganate), $MnSO_4{\cdot}4H_2O$ (manganese sulphate tetrahydrate), $AgNO_3$ (silver Nitrate) and HNO_3 (nitric acid) were used in study.

2.2. Material synthesis

The Ag doped OMS-2 catalyst was synthesized using the reflux method. Solution A was prepared by mixing 30 ml of 0.5 mol l^{-1} $MnSO_4{\cdot}H_2O$ solution with few drops of concentrated HNO_3 at room temperature to provide an aqueous solution of pH 1. Solution B was made by mixing 0.03 mole of $KMnO_4$ and 0.0011 mole of $AgNO_3$ in 100 ml water. Thereafter, solution A was added dropwise into solution B. The resultant black precipitate was stirred dynamically and refluxed at 373 K for 48 h. Solid formed in the solution was filtered and washed using distilled water and kept for drying at 383 K followed by calcination at 573 K in static air for 5 h. The obtained dark brown powder was Ag Doped OMS-2.

2.3. Characterization

Field emission scanning electron microscope (FESEM) micrographs of Ag-OMS-2 nanorods was taken on JEOL's JSM-7800F at 10 KeV beam energy. The elemental analysis of nanorods was performed using energy dispersive x-ray spectroscopy (EDX) in FESEM. Structural investigations of nanorods were performed by high resolution transmission microscope (HRTEM) using 200 keV beam energy. Crystal structure of the Ag-OMS-2 was determined by x-ray diffraction (XRD) using CuKα radiations of 5418 Å wavelength source.

2.4. Sensor device fabrication

An insulated substrate with gold coated copper electrodes was taken for the fabrication of the sensor. As shown in figures 1(a)–(d), two linear electrodes of copper were fabricated on a copper clad printed circuit board using photolithograph. Electrodes dimensions were kept at 2 cm × 0.3 cm (Length x width) with an interelectrode gap of 0.3 cm. In order to enhance the resistance and prevent the oxidation, Cu electrodes were electroplated using gold (figures 1(b), (c)). The respective thickness of Cu electrodes and Au film coating was kept 8 μm and 0.1 μm, respectively. The sensor film was deposited on the electrodes using the drop cast method and the dimensions of the sensor film was controlled by a hard mask figures 1(b), (e)).

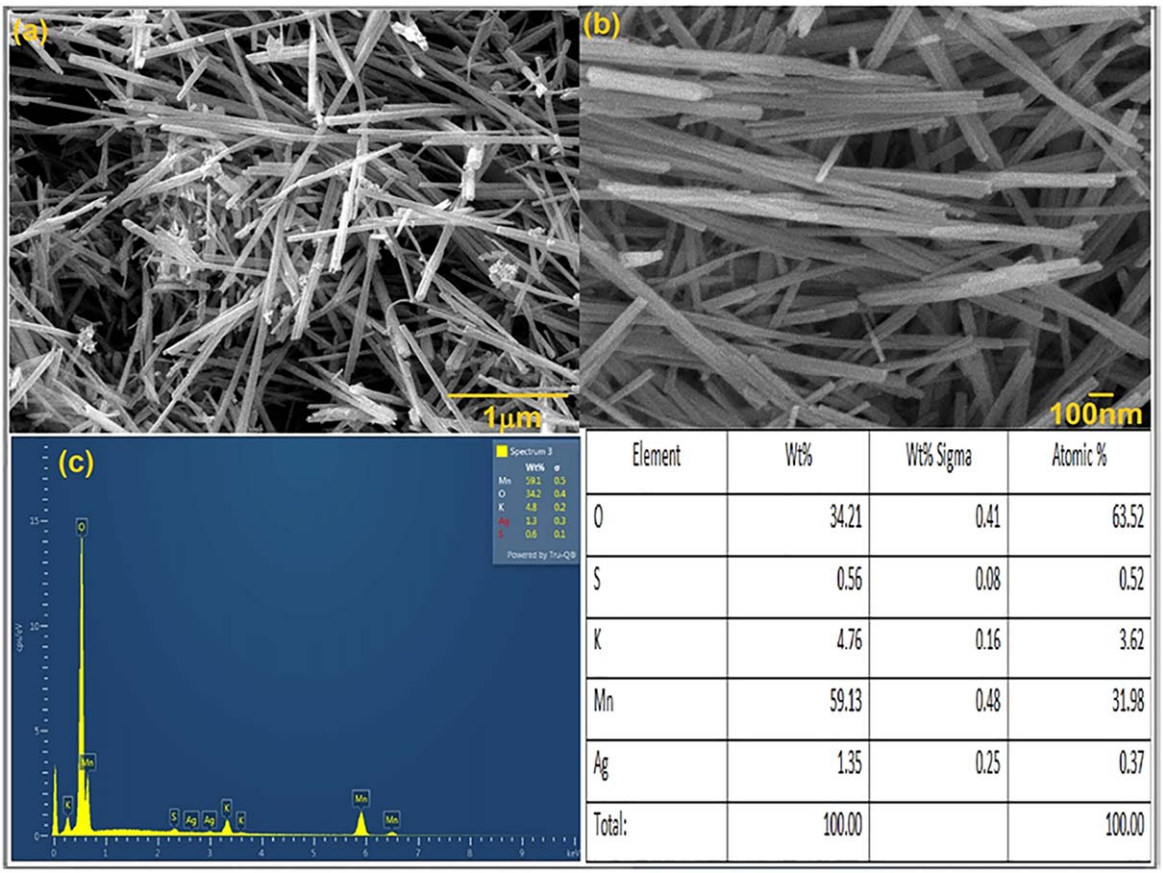

Element	Wt%	Wt% Sigma	Atomic %
O	34.21	0.41	63.52
S	0.56	0.08	0.52
K	4.76	0.16	3.62
Mn	59.13	0.48	31.98
Ag	1.35	0.25	0.37
Total:	100.00		100.00

Figure 2. (a) SEM micrographs displaying the fiber shaped morphology of Ag-OMS-2 (b) magnified SEM micrograph of Ag-OMS-2 fibers (c) EDX spectra of fibers (d) table showing the weight (wt) % and atomic (at.) % of different elements in fibers.

Ag-OMS-2 nanorods weighing 0.23 g, were dispersed in 0.1 ml of ethanol and solution was sonicated for 30 min. Thereafter, material was drop casted between the electrodes in the form of a thin film (∼15 μm thickness) and left for a while (figure 1(a)). To remove solvent and to make film stable, the sensor device was kept in a convection oven for 6 h at 80 °C. So formed sensor showed a stable electrical resistance of 557 kΩ in air at room temperature which confirmed the stable contact formation amid electrodes and sensor film.

2.5. Gas sensing measurements

An indigenous gas sensor system was used to study the behaviour of sensor device towards presence and absence of gas molecules. As shown in figure 1(b), it is a gas chamber with sample holder, in-built heater and gas inlet and outlet. The film of the sensor was positioned inside the chamber and the resistance change of sensor in the presence/absence of the CO gas was examined by a datalogger. Sigma gas cylinder was used for dry CO gas integrated with MFC to control the flow rate and concentration of CO gas in gas chamber.

The base resistance of the sensor device was acquired at room temperature (30 °C) with ∼45% relative humidity in air. The variations in the resistance of the sensor in the presence/absence of CO gas were observed and recorded by a multimeter (SUKam) data logger. The sensor response S% was calculated by equation (1) [25–27].

$$S\% = \frac{(Ra - Rg)\times 100}{Ra} \quad (1)$$

Here, resistance of sensor film R_a in air and R_g in the presence of CO gas in air.

3. Results and discussion

3.1. Characterization of Ag-OMS-2 nanorods

Figure 2(a) shows the FESEM micrograph of as-prepared Ag-OMS-2 nanorods in diverse dimensions. Magnified image of fibers in figure 2(b) shows the needle like appearance with average 20 nm diameter.

Various peaks in EDX graph of elements in figure 2(c) show the presence of Ag, K, O and Mn elements in the fibers. Quantitative analysis in table in figure 2(d) reveals the occurrence of 31.98 at.% Mn and 63.52 at.% O are the major elements and K with 3.62 at.% is a minor element in the Ag-OMS-2 nanorods. EDX analysis also shows presence of 0.37 at.% Ag because of doping in the nanorods.

HRTEM micrograph in figure 3(a) demonstrates a bunch of Ag-OMS-2 nanorods. Presence of crystalline structure in nanorods is shown by the high magnification micrographs two nanorods in figure 3(b). X-ray diffraction peaks of Ag-

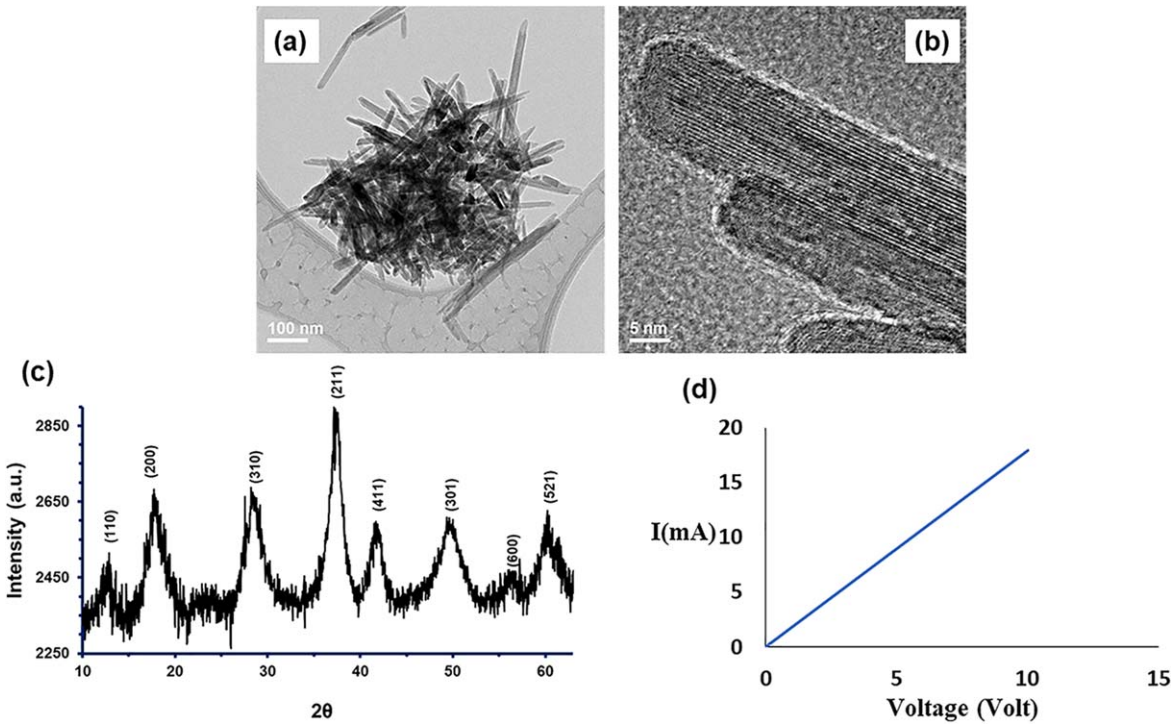

Figure 3. High resolution transmission electron micrographs showing (a) Ag-OMS-2 nanorods in a bunch (b) section of two Ag-OMS-2 nanorods in high magnification (c) x-ray diffraction of Ag-OMS-2 (d) Current voltage behaviour of Ag-OMS-2 nanorods.

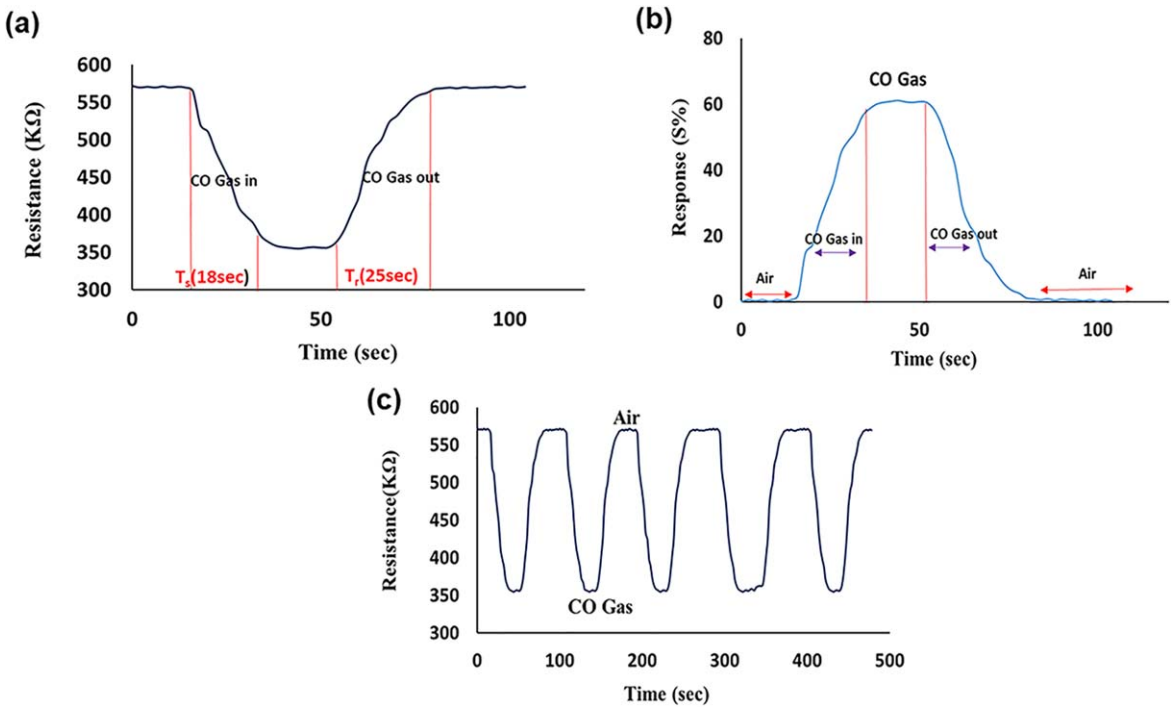

Figure 4. Change in (a) resistance and (b) response of Ag-OMS-2 after exposure to 100 ppm of carbon monoxide gas (c) variation in sensor film resistance throughout CO gas exposure and recovery after removal of gas source in five cycles.

OMS-2 nanorods in figure 3(c) are at the same positions as in K-OMS-2, described in previous studies [23, 28]. This shows that the doping of Ag in K-OMS-2 do not change its crystal structure.

3.2. Electrical properties of Ag-OMS-2 fibers

Figure 3(d) displays the voltage current (V-I) of Ag-OMS-2 nanorods at room temperature (32 °C) Graph shows that the current increases linearly with the increase in the in Ag-OMS-

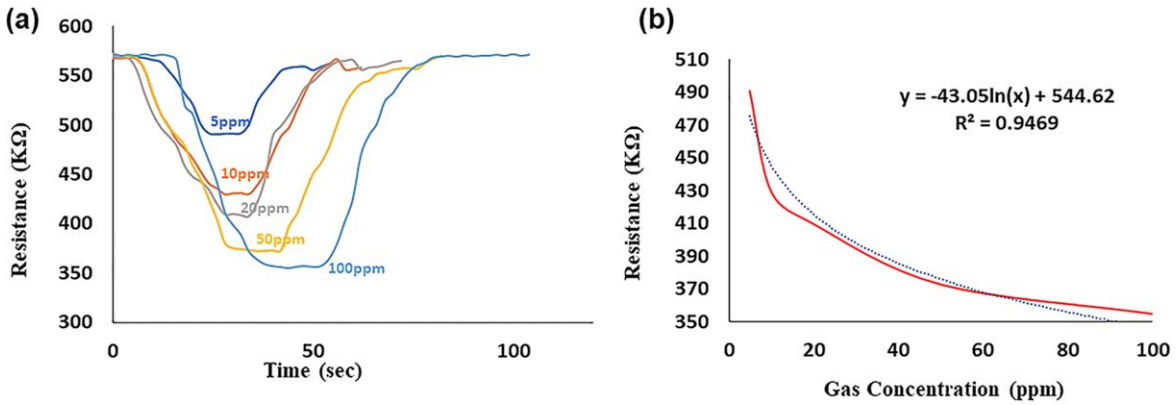

Figure 5. (a) Variation in resistance of Ag-OMS-2 film during exposure to various concentrations of CO gas ranging from 5 ppm to 100 ppm and subsequent recovery (b) calibration curve for CO gas concentrations.

2 nanorods. This also confirms the stable contact formation between sensor film and electrodes.

3.3. Response of Ag-OMS-2 towards CO

As shown in figure 4(a), the resistance of the Ag-OMS-2 film drops from 557 kΩ to 352 kΩ in 18 sec, after it was exposed to 100 ppm of CO (carbon monoxide) gas. After the removal of CO gas source from chamber, the film regained its initial resistance to 557 kΩ in 25 sec. As displayed in figure 4(b), saturation in the response of sensor film was noticed after ∼18 s after reaching to 61%. It remained stable at that value until the CO gas was present in the chamber. It was retrieved to 0% after removal of CO gas source. A minute noise is detected during the exposure of Ag-OMS-2 film to carbon monoxide gas. This might be ascribed to the effect of CO molecules impacting on the sensor film and/or impact of intrusive gases found in the air. Yet, the highest response detected due to noise was ∼1% which is insignificant in contrast to 61% response for 100 ppm CO gas.

Figure 4(c) displays five uninterrupted cycles of variation in electrical resistance during the exposure of Ag-OMS-2 film to 100 ppm CO gas and its recovery after removal of gas source. Study reveals that the response of material is sustained during recurring cycles of CO gas introduction and exclusion from the chamber.

Figure 5(a) demonstrates the dynamic gas sensing and recovery of Ag doped OMS-2 nanorods with various concentration of CO gas ranging from 5 ppm to 100 ppm. The response to sensing and recovery differ in reversible style as chamber gas is swapped from air to carbon monoxide and conversely. Study also reveals that the sensor film revisited the zero response for every concentration of CO gas during retrieving in air. The figure 5(b) shows calibration curve of sensor with respect to CO gas concentration showing regression value (R) of 0.94.

As 5–20 ppm concentrations are significantly lower than the danger level of 35 ppm, Ag-OMS-2 is highly appropriate for the detection of CO gas. Sensor showed good response of 13% for 5 ppm CO gas. The response increased to 61% when the CO gas concentration was increased to 100 ppm respectively.

3.4. Stability of Ag-OMS-2 and its response and selectivity for CO gas

The sensor Ag-OMS-2 film displayed steady electrical and sensing parameters for the period of three months. As displayed in figure 6(a), small variation in the response of sensor film for 100 ppm of CO gas from 61 to 58% was observed during the initial 30 days. However, after 30 days to 90 days the response was reduced from 61% to 52% in various intervals.

Selectivity of the sensor film for CO gas was established by exposing the sensor film to oxygen, carbon dioxide, nitrogen, ammonia, nitrogen dioxide, hydrogen disulfide, carbon monoxide gases (>500 ppm) and volatile organic compounds (VOC) vapors e.g., ethanol, methanol, and xylene (200 ppm), at 28 °C. In addition, the sensor film response to 65% humidity was too examined. As displayed in figure 6(b), response of sensor film was <2% for gases and VOC vapors excluding carbon monoxide and humidity. The response of the sensor film for CO gas is three times (>60%) in comparison to <20% for humidity.

3.5. Effect of relative humidity (RH) on the response to CO gas

Figure 6(c) shows the effect of relative humidity on the response of sensor film for 100 ppm CO gas. Sensors displayed slight changes in the response 30% to 70% relative humidity of However, effect of humidity increases much faster beyond 65% RH. This might be because of the barrage of active sites over the catalysts surface. As demonstrated in previous studies [29], excess humidity alters the oxidation reaction of CO in comparison to dry conditions. At the low humidity level, H_2O can barrage the active sites for CO adsorption on the Ag-OMS-2 surface which decreases the sensing capability of the Ag-OMS-2 for CO gas.

3.6. Comparison of Ag-OMS-2 with reported CO gas sensors studies

Sensing activity comparison of Ag-OMS-2 with other reported CO gas sensor studies in literature is given in table 1. Top 6 materials in the table 1 [30–35] works at higher operating temperatures (>175 °C) whereas other sensor materials

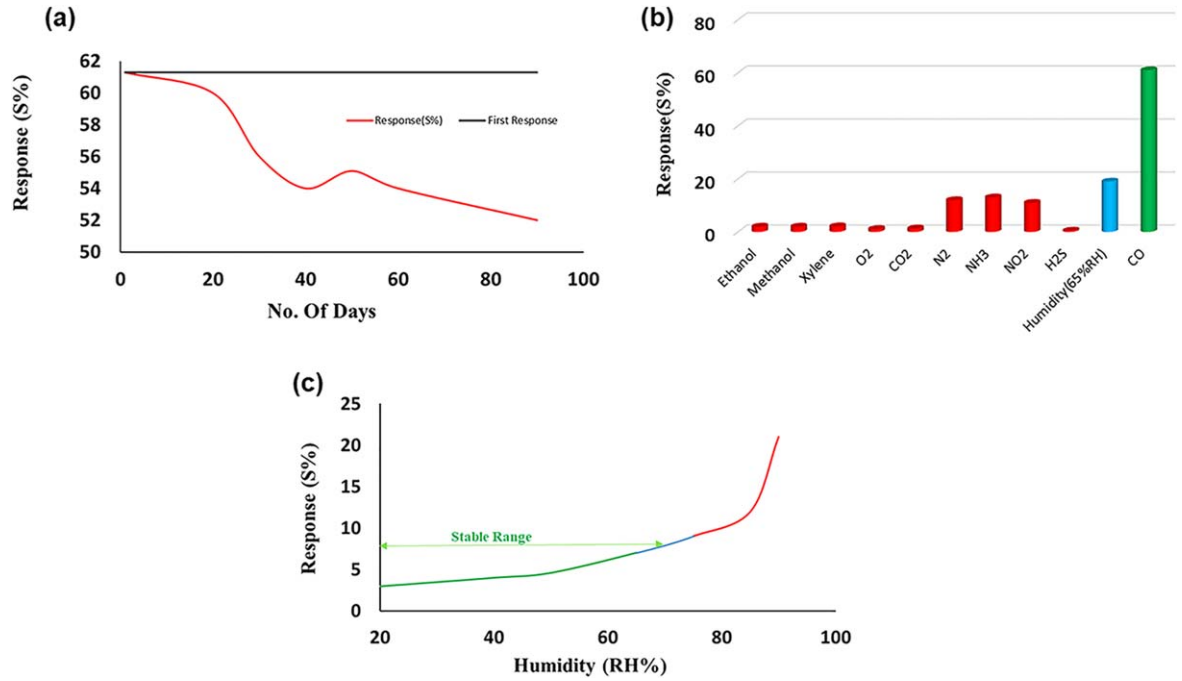

Figure 6. (a) Variation in the response of AgOMS-2 film with time to 100 ppm CO gas during 90 days (b) Response from the sensor film when exposed to oxygen, carbon dioxide, nitrogen, ammonia, nitrogen dioxide and hydrogen disulfide gases, vapors of ethanol, methanol and xylene, at 200 ppm concentration, and 65% RH (c) Variations in the response of Ag-OMS-2 for CO gas with the change in relative humidity (RH%).

Table 1. Sensing activity comparison of Ag-OMS-2 with other reported CO gas sensor studies in literature.

S.no	Sensor material for CO gas sensing	Working temp	Gas amount (ppm),	Response time	Response 'S'	References
1	stabilized ZrO_2	873 K	100 ppm	10s	90%	[30]
2	SnO_2 nanosheets	673 K	50 ppm	6s	~1.5	[31]
3	Au-decorated SnO_2 nanobelt	523–673 K	10 ppm	30s	90%	[32]
4	ZnO nanowire	593 K	500 ppm	100s	60%	[33]
5	ZnO nanowire with Au nanoparticles	593 K	100 ppm	40s	53%	[34]
6	Spinel-perovskite composite sensor	448K	250 ppm	300s	~75%	[35]
7	Pd-decorated In_2O_3 nano bundle	300 K	100 ppm	50s	85%	[36]
8	Pt Loaded SnO_2 PNS	300 K	100 ppm	144s	~64.5%	[37]
9	Cu-OMS-2	296 K	10 ppm	60s	20%	[23]
10	Nb-OMS-2	296K	10 ppm,	40s	32%	[22]
11	Ag-OMS-2 (Present study)	300K	10 ppm	28s	*24.5%*	Present work

including present study [22, 23, 36, 37] works at room temperature for CO gas sensing. Although the response time of first 5 sensors for CO gas is short with good response but sensing temperature is high. For example, Qian *et al* [32] showed that Au decorated SnO_2 nano belt takes only 30 s for sensing of 10 ppm CO gas but only at 573–673 K temperature. SnO_2 nanosheets [31] takes only 6s for 50 ppm CO gas but at 673 K.

Among 5 sensor materials which works at room temperature, three of them are metal doped OMS-2. Other two materials, Pd-decorated In_2O_3 nano bundles and Pt based sensors [36, 37] are costly sensor materials. Pt Loaded SnO_2 PNS. shows longer response time. Ag-OMS-2 sensor film takes 28 s for 10 ppm CO gas at room temperature which is better than the other two OMS-2 based sensors in terms of response time which is 60 sec and 28sec for Cu-OMS-2 and Nb-OMS-2 respectively.

3.7. Proposed mechanism of CO sensing by Ag- OMS-2

Superior activity of Ag-OMS-2 for CO gas sensing at low (300K) temperature is supported by its tunnel structure and nanorod morphology which led to the swift activation of oxygen molecules for the oxidation of CO gas. A pictorial presentation of proposed Sensing mechanism of CO gas by Ag-OMS-2 is shown in figure 7.

It was proposed in earlier studies that the Ag–O–Mn bridge in Ag–OMS-2 structure opens the pathway for the free electron transfer between MnOx and Ag which led towards the higher mobility and activeness of bridged oxygen, giving rise to enhanced activity for CO oxidation [24, 38]. Hu *et al* [39] also reported that diffusion of lattice oxygen species and higher CO adsorption caused by doping K–OMS-2 with Ag +, supporting the CO oxidation.

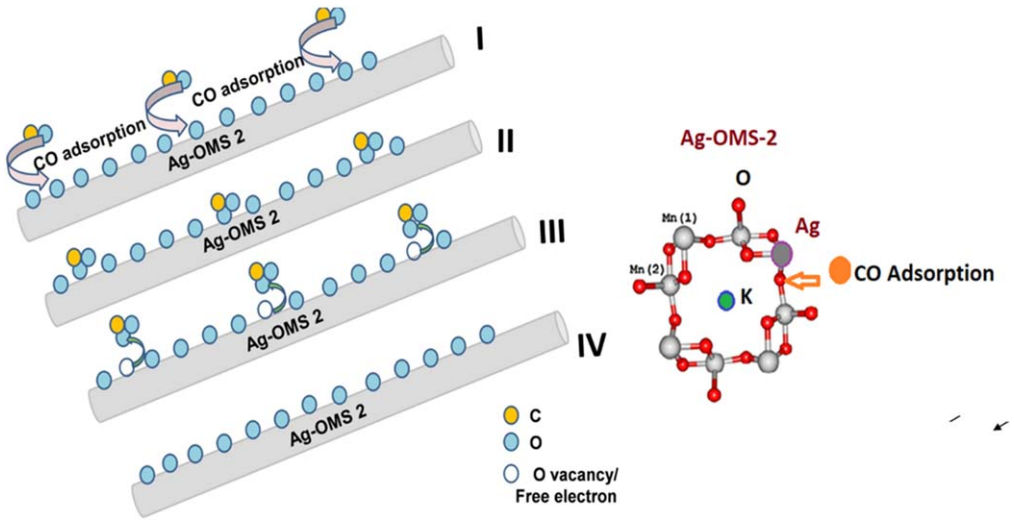

Figure 7. Proposed mechanism for adsorption and desorption of CO on Ag-OMS-2,1st step: CO adsorption on Ag-OMS-2, IInd: CO conversion to CO_2 after taking the oxygen from OMS-2 surface, IIIrd step: leaving of CO_2 from Ag-OMS-2 surface leaving an oxygen vacancy, IVth step: replenishing of oxygen on the surface of material by atmospheric oxygen.

For the Ag–OMS-2 nanorods, smooth activation and conversion of oxygen species amid silver present in the tunnel and manganese oxide, connoted by the facile reduction feature on the Ag–OMS-2. On reactive sites the adsorbed CO converts into CO_2 after oxidizing by the oxygen species provided by OMS-2 in the first and second steps (figure 7). This gives rise to free electrons resulting in to increase in current and decrease in resistance. This also creates the oxygen vacancy in the Ag-OMS-2 which is replenished by oxygen from the atmosphere. The free electrons replaced by the oxygen species and resistance starts increasing to initial levels.

4. Conclusion

A thin film-based gas sensor for the detection of CO with employing Ag doped octahedral molecular sieves (Ag-OMS-2) nanorods has been developed. The sensor specifically adsorbs and desorbs CO gas, moreover the other notable specifications are its rapid response time (18s), recovery time (25s) for 100 ppm CO gas at room temperature, it operates within reasonably low range (5–100 ppm), and also displayed stability of over 8 months. This study could unlock the pathways for the evolution of more advanced CO gas sensors operating at room temperature.

Acknowledgments

Support of this study is provided by the SERB, India via Grant TAR/2021/000407 is gratefully acknowledged. We are grateful to C4FED, IIT, Mandi, India for support in characterisation of materials.

References

[1] Duong V T, Nguyen C T, Luong H B, Luu L A, Nguyen D C and Nguyen H 2019 *Adv. Nat. Sci.: Nanosci. Nanotechnol.* **10** 015001
[2] Tran Q T, Huynh T M, Tong D T and Nguyen N D 2013 *Adv. Nat. Sci.: Nanosci. Nanotechnol.* **4** 045012
[3] Hien V X 2018 *Adv. Nat. Sci.: Nanosci. Nanotechnol.* **9** 045013
[4] Nguyen D D, Do D T, Vu X H, Dang D V and Nguyen D C 2016 *Nanosci. Nanotechnol.* **7** 015004
[5] Nguyen D D, Dang D V and Nguyen D 2015 *Adv. Nat. Sci.: Nanosci. Nanotechnol.* **6** 035006
[6] Rauba J A, Nolf M M, Hampson N B and Thom S R 2000 *Toxicology.* **145** 1
[7] Jaiswal M, Majumdar N, Kumar R, Mittal J and Jha P 2022 *Adv. Nat. Sci.: Nanosci. Nanotechnol.* **13** 043002
[8] Yamazoe N and Miura N 1995 *IEEE Trans. Compon. Packag. Manuf. Technol.* A **18** 252
[9] Seal S and Shukla S 2002 *JOM* **54** 35
[10] Biabani-Ravandi A, Rezaei M and Fattah Z 2013 *Chem. Eng. J.l.* **219** 124
[11] Zhao K, Tang H, Qiao B, Li L and Wang J 2015 *ACS Catal.* **5** 3528–39
[12] Pahalagedara L *et al* 2017 *Appl. Catal.* B **204** 411
[13] Kumar R, Kumar R, Kushwaha N and Mittal J 2016 *IEEE Sens. J.* **16** 4691
[14] Yang J, Zhou H, Wang L, Zhang Y, Chen C, Hu H, Li G, Zhang Y, Ma Y and Zhang J 2017 *ChemCatChem* **9** 1163
[15] Genuino H C, Meng Y, Horvath D T, Kuo C H, Seraji M S, Morey A M, Joesten R L and Suib S L 2013 *ChemCatChem* **5** 2306
[16] Chen J, Li J, Li H, Huang X and Shen W 2008 *Microporous Mesoporous Mater.* **116** 586
[17] Hu B, Chen C H, Frueh S J, Jin L, Joesten R and Suib S L 2010 *J. Phys. Chem.* C **.114** 9835
[18] Wasalathanthri N D *et al* 2019 *RSC Adv.* **9** 32665–73
[19] Jothiramalingam R, Viswanathan B and Varadarajan T K 2006 *J. Mol. Catal. A: Chem.* **252** 49
[20] Kumar R, Kushwaha N, Pandey S, Priya R and Mittal J 2018 *IEEE Sens. J.* **18** 956

[21] Peluso M A, Gambaro L A, Pronsato E, Gazzoli D, Thomas H J and Sambeth J E 2008 *Catal. Today* **133-135** 487
[22] Kumar R, Jaiswal M, Singh O, Gupta A, Ansari M S and Mittal J 2019 *IEEE Sens. J.* **19** 7201
[23] Kumar R, Mittal J, Kushwaha N, Rao B V, Pandey S and Pu Liu C 2018 *Sens Actuat B. Chem.* **266** 751
[24] Xia G G, Yin Y G, Willis W S, Wang J Y and Suib S L 1999 *J. Catal.* **185** 91
[25] Kumar R, Kushwaha N and Mittal J 2017 *Sens. Actuat. B: Chem.* **244** 243
[26] Jaiswal M, Kumar R, Mittal J and Jha P 2020 *Sens Actuat B: Chem* **310** 127826
[27] Jaiswal M, Kumar R, Mittal and Jha P 2022 *IEEE Sens. J.* **22** 6303
[28] King'ondu C K, Opembe N, Chen C, Ngala K, Huang H, Iyer A, Garcés H F and Suib S L 2011 *Adv. Funct. Mater.* **211** 312–23
[29] Hernández W Y, Centeno A, Ivanova S, Eloy P, Gaigneaux E M and Odriozola J A 2012 *Appl Catal B Environ* **123** 27
[30] Miura N, Raisen T, Lu G and Yamazoe N 1998 *Sens. Actuat B: Chem.* **1** 84
[31] Moona C S, Kima H R, Auchterlonie G, Drennan J and Lee J H 2008 *Sens. Actuat B Chem* **131** 556
[32] Qian L H, Wanga K, Lia Y, Fang H T, Lua Q H and Maa X L 2006 *Mater. Chem. Phys.* **100** 82
[33] Harsh T J, Chenb Y W, Changa S J, Wang S F, Hsuc C L, Lin Y R, Lin T S and Chene I C 2007 *Sens. Actuat B Chem.* **125** 498
[34] Chang S J, Hsueh T J, Chen I C and Huang B R 2008 *Nanotechnology* **19** 175502
[35] Maity A, Ghosh A and Majumder S B 2016 *Sens. Actuat Chem* B **225** 128
[36] Lai H Y and Chen C H 2012 *J. Mater. Chem.* **22** 13204
[37] Wanga K, Zhaoa T, Liana G, Yua Q, Luana C, Wangb Q and Cuia D 2013 *Sens. Actuat* B **184** 33
[38] Gac W 2007 *Appl. Catal.* B **75** 107
[39] Hu R R, Yi C, Xie L Y and Wang D Z 2007 *Chin. J. Catal.* **28** 463